nanoenergy advances

MDPI

Review

Measuring Physical and Chemical Properties of Single Nanofibers for Energy Applications—Possibilities and Limits

Tomasz Blachowicz [1], Nonsikelelo Sheron Mpofu [2,3] and Andrea Ehrmann [2,*]

[1] Institute of Physics—Center for Science and Education, Silesian University of Technology, 44-100 Gliwice, Poland; tomasz.blachowicz@polsl.pl
[2] Faculty of Engineering and Mathematics, Bielefeld University of Applied Sciences and Arts, 33619 Bielefeld, Germany; nonsiempofu@gmail.com
[3] School of Engineering, Moi University, Eldoret 30100, Kenya
* Correspondence: andrea.ehrmann@hsbi.de

Abstract: Nanofibers can be produced by various techniques, such as a broad range of electrospinning techniques to produce nanofiber mats from different polymers or polymer blends, often filled with metallic or semiconducting nanoparticles or by different nanotechnological bottom-up or top-down methods. They are important parts of a wide variety of energy applications, such as batteries, fuel cells, photovoltaics, or hydrogen storage materials. Usually, their physical or chemical parameters are measured by averaging over a fiber bundle or a part of a nanofiber mat. Here, we report the possibility of measuring the different physical and chemical properties of single nanofibers and nanowires. Such measurements of single nanofiber properties are more complicated than investigations of fiber bundles or whole nanofiber mats and, thus, are less often found in the literature. After a fast increase in such investigations between 2001 and 2009, the numbers of respective studies are now stagnating. This review thus aims to make the different possibilities more visible to a broader scientific audience by providing several examples based on atomic force microscopy (AFM) and other broadly available techniques. The focus of this review is on technologies that reveal more information than the pure surface morphology of nanofibers or nanowires, such as mechanical properties or wettability, porosity, or electrical conductivity.

Keywords: nanofiber; nanowire; electrospinning; energy applications; atomic force microscopy (AFM)

Citation: Blachowicz, T.; Mpofu, N.S.; Ehrmann, A. Measuring Physical and Chemical Properties of Single Nanofibers for Energy Applications—Possibilities and Limits. *Nanoenergy Adv.* **2024**, *4*, 300–317. https://doi.org/10.3390/nanoenergyadv4040018

Academic Editors: Carmen M. Rangel, Joao Ventura and Elby Titus

Received: 5 August 2024
Revised: 20 September 2024
Accepted: 27 September 2024
Published: 9 October 2024

1. Introduction

Nanofibers and nanowires are nowadays used for a wide variety of applications, from sensing [1,2] to filtration [3,4], from biomedicine [5,6] to energy applications [7,8].

Nanofibers are often produced by electrospinning, enabling the creation of nanofiber mats with aligned or arbitrarily distributed nanofiber from diverse polymers, polymer blends, and included nanoparticles [9–11]. Such polymeric nanofiber mats can be carbonized to prepare carbon nanofibers [12–14], or even pure ceramic or metallic fibers can be produced by calcination of the polymeric part of composite fibers [15–17]. Other processes, such as enzyme-mechanical preparation of cellulose nanofibers, are usually applied only for specific materials [18–20].

In many cases, these nanofiber mats are investigated as a whole, e.g., measuring the average fiber diameter on a defined area of an electrospun nanofiber mat. Only a few studies aim at measuring the physical or chemical properties of single nanofibers or nanowires, as Figure 1 shows. This review collects the methods for single-fiber investigations reported in the scientific literature and provides an overview of their possibilities and limits.

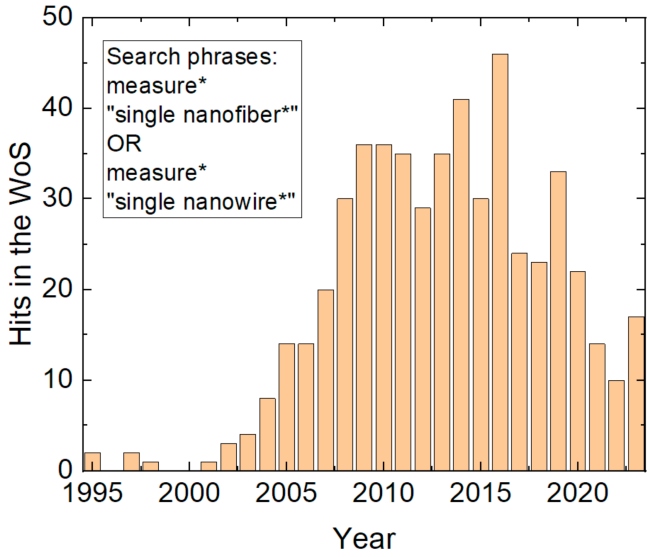

Figure 1. Hits in the Web of Science for the indicated search phrases (data collected on 14 July 2024).

2. Nanofibers in Energy Applications

Nanofibers can be used in diverse energy applications [21,22]. Often, conductive nanofibers, i.e., typically carbon nanofibers (CNFs), are used here, either alone or doped with diverse nanomaterials [23]. Supercapacitors can be used as electrodes, where a high surface area and good wettability are important parameters for high capacitance and good cycle stability [24,25]. Such a high specific surface area as well as high total volume can be obtained, e.g., by NaOH activation and subsequent carbonization of SiCNO nanofibers at optimized temperatures [26]. Alternatively, CNFs can be used in composite electrodes with a large surface area [27]. It should be mentioned that while high porosity and surface area are generally found to be advantageous for nanofibers in energy applications, mechanical robustness also has to be taken into account [28].

In fuel cells, CNFs can be used as catalyst carriers to reduce the necessary amount of Pt or similar materials [29]. Here, charge transfer is a crucial parameter and thus conductivity in single nanofibers as well as at the crossing points [30].

Diverse battery types use carbon nanofibers, such as lithium-ion batteries (LIBs), Na ion batteries (NIBs), K-ion batteries (KIBs), etc. [21]. Here again, the porosity, the accessible surface area, and the conductivity have been found to play an important role [31,32]. In electrostatic capacitors, composites filled with $Ba_{0.6}Sr_{0.4}TiO_3$ nanofibers were found to be well-suitable dielectrics, reaching high energy storage efficiency [33].

Besides these energy-storing applications in rigid or flexible electronics [34], diverse applications in energy harvesting or conversion are reported in the literature. In hydrogen production by electrochemical hydrogen reaction (HER), CNFs can be used due to their high electronic conductivity, enabling high electrocatalytic activity [35]. Mechanical energy harvesting by a triboelectric nanogenerator (TENG) is often studied using composites containing CNFs of other conductive nanofibers, such as polyvinylidene fluoride (PVDF)/graphene, whose conductivity and surface structure are crucial for the charge collection and transfer [36–39]. With perovskite/PVDF nanofiber composites, triboelectric and piezoelectric energy harvesting can be combined [40]. Using CNT/PEDOT:PSS conductive nanofibers, the thermoelectric effect was used for human body energy harvesting [41]. Mesoporous carbon nanowires or graphene oxide (GO)/cellulose nanofibers have also been used for osmotic energy conversion [42,43].

Based on these studies, important parameters of nanofibers and nanowires are their morphology, especially the porosity, conductivity, wettability, and mechanical properties.

3. Measuring the Morphology of Single Nanofibers

While the morphology of nanofiber mats is regularly investigated in diverse studies, there are also many reports of the morphology, i.e., surface structure and porosity, of single nanofibers. Depending on the required resolution, the methods can coincide. While normal optical microscopy is not suitable for nanofiber mats, confocal laser scanning microscopy (CLSM) can often be used to visualize nanofiber mats if the single nanofibers are not too thin [44–46]. The maximum lateral resolution of a CLSM is in the range of 140–200 nm [47,48], depending on the wavelength of the used laser and the numerical aperture of the used lens, making this technology useful for an overview of the nanofiber orientation. Measuring the nanofiber diameters, however, is limited to such nanofibers with sufficiently large diameters since thinner ones are not visible in CLSM images and will necessarily result in a larger error than measurements with higher resolution.

Amongst the latter, typical methods to investigate whole nanofiber mats are scanning electron microscopy (SEM), transmission electron microscopy (TEM), and atomic force microscopy (AFM), with resolutions depending on the used instruments and also on the sample surfaces [49]. SEM images are especially often shown in reports of diverse nanofiber mats. While they are often used to measure nanofiber diameters [50–52], high-quality SEMs can also investigate the fiber surface to a certain degree [53], as well as integrated nanoparticles [54]. Some examples of such high-resolution SEM images are given in Figure 2.

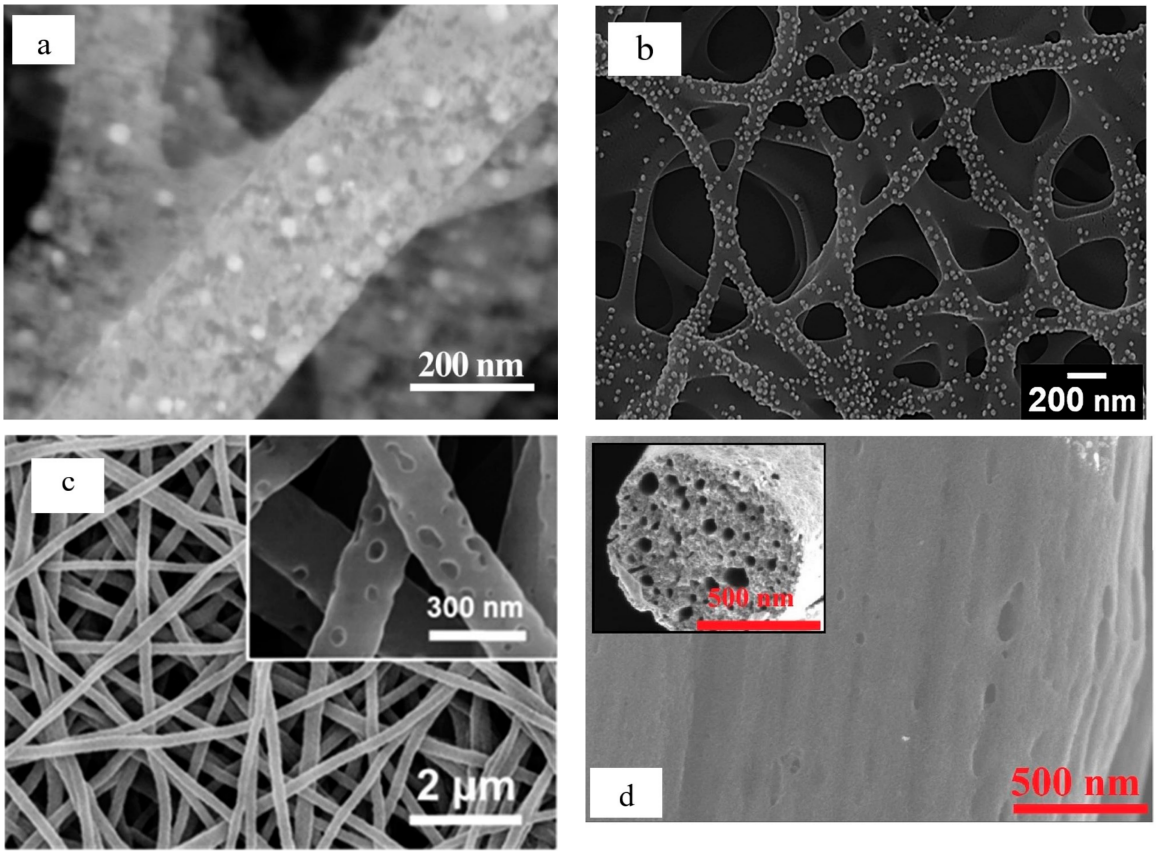

Figure 2. Scanning electron microscopy (SEM) images of nanofibers. (**a**) carbon nanofibers with uniformly dispersed Fe/Co alloy nanoparticles, reprinted with permission from [54], Copyright 2021, Elsevier; (**b**) Au nanoparticles on graphene oxide (GO) nanofibers, reprinted with permission from [55], Copyright 2020, Elsevier; (**c**) porous carbonized poly(acrylonitrile) (PAN)/poly(vinyl pyrrolidone) (PVP) nanofibers, reprinted with permission from [56], Copyright 2020, Elsevier; (**d**) surface and porous cross-section of activated carbon nanofibers, nitrogen-doped in the presence of Ni foil, reprinted with permission from [57], Copyright 2020, Elsevier.

Higher resolutions are enabled by TEM and AFM images. TEM allows for investigating nanoparticles not only in the nanofibrous membranes [58] but also inside the nanofibers themselves [59–61]. At the same time, TEM can, in principle, be performed on parts of nanofiber mats or fiber bundles [62]. Very often, only single fibers are shown, and authors should carefully avoid "cherry-picking" those parts of such nanofibers that best fit the intended message [62]. It should be mentioned that sample preparation for TEM is much more complicated than for many other techniques. Single fibers can, e.g., be dispersed in isopropyl alcohol or in acetone, possibly ultrasonicated and drop-casted on a holey carbon grid [58]. Alternatively, fibers can be inserted in acetone, transmit resin, polymerized, and cut by an ultra-microtome to get thin slices [62]. Exemplary TEM images of single nanofibers with nanoparticles or pores are depicted in Figure 3.

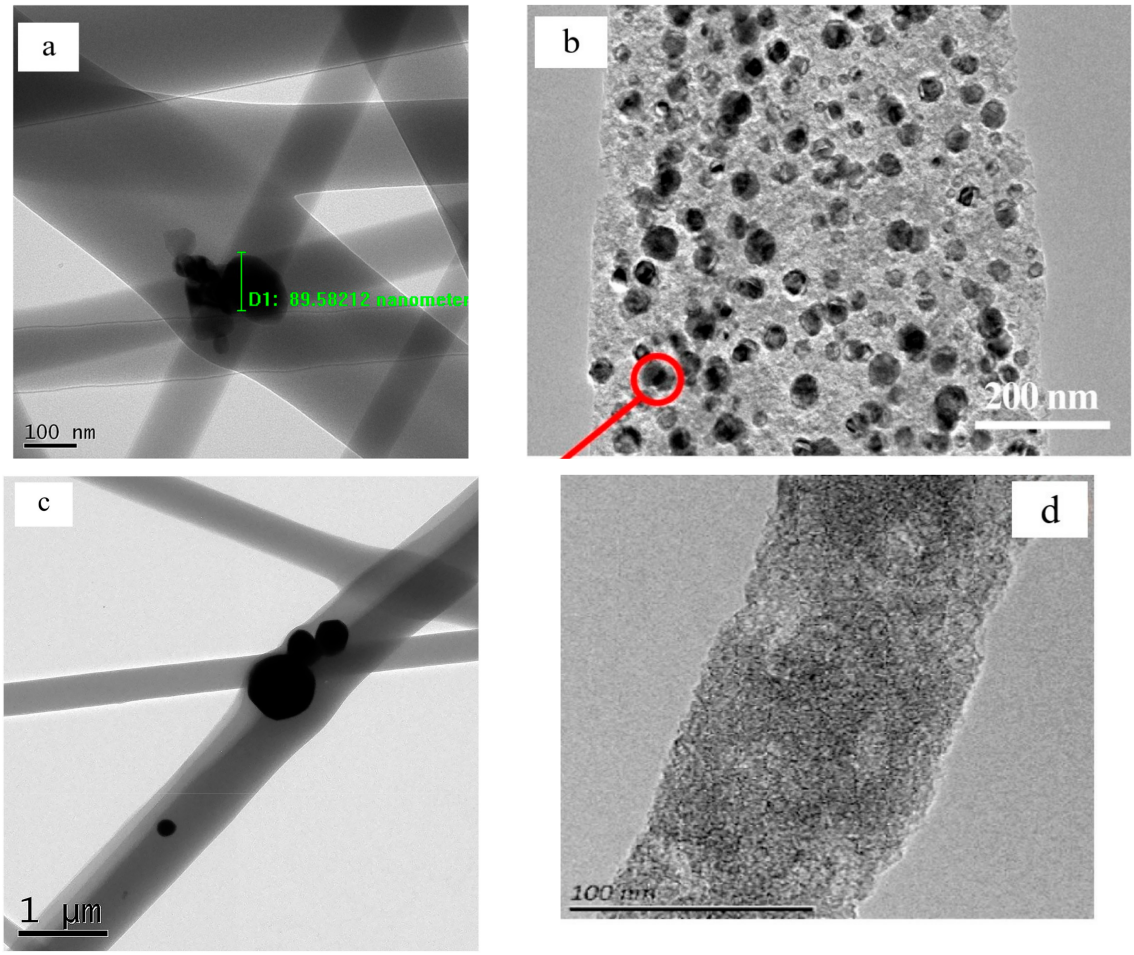

Figure 3. Transmission electron microscopy (TEM) images of nanofibers. (**a**) ZnO nanoparticles in poly(vinyl alcohol) (PVA) nanofibers, from [28], originally published under a CC BY license; (**b**) carbon nanofibers with uniformly dispersed Fe/Co alloy nanoparticles, reprinted with permission from [54], Copyright 2021, Elsevier; (**c**) Janus nanofiber with EC-Ag nanoparticles on one side and PVP on the other side; reprinted with permission from [63], Copyright 2020, Elsevier; (**d**) porous cellulose acetate-based carbon nanofiber, reprinted with permission from [64], Copyright 2022, Elsevier.

AFM has another advantage besides the high resolution and the possibility to easily measure the roughness of single nanofiber surfaces [65,66], that is, the option to detect material differences, measure elastic properties, etc., in addition to the surface morphology [66]. The disadvantage, on the other hand, is the overestimation of nanofiber diameters due to the AFM tip radius, which broadens the apparent diameter and the elastic displacement of nanofibers in the scan direction [49]. Generally, the touching measurement method—even in the so-called non-contact or tapping mode—often results in measurement errors due to

erroneous fiber movements, and generally, objects with relatively large height: width ratio, such as nanofibers, will lead to less sharp images due to the required AFM settings [67]. Some exemplary AFM images of fiber morphologies are depicted in Figure 4, including a phase image in which height changes are better visible than in standard topography maps.

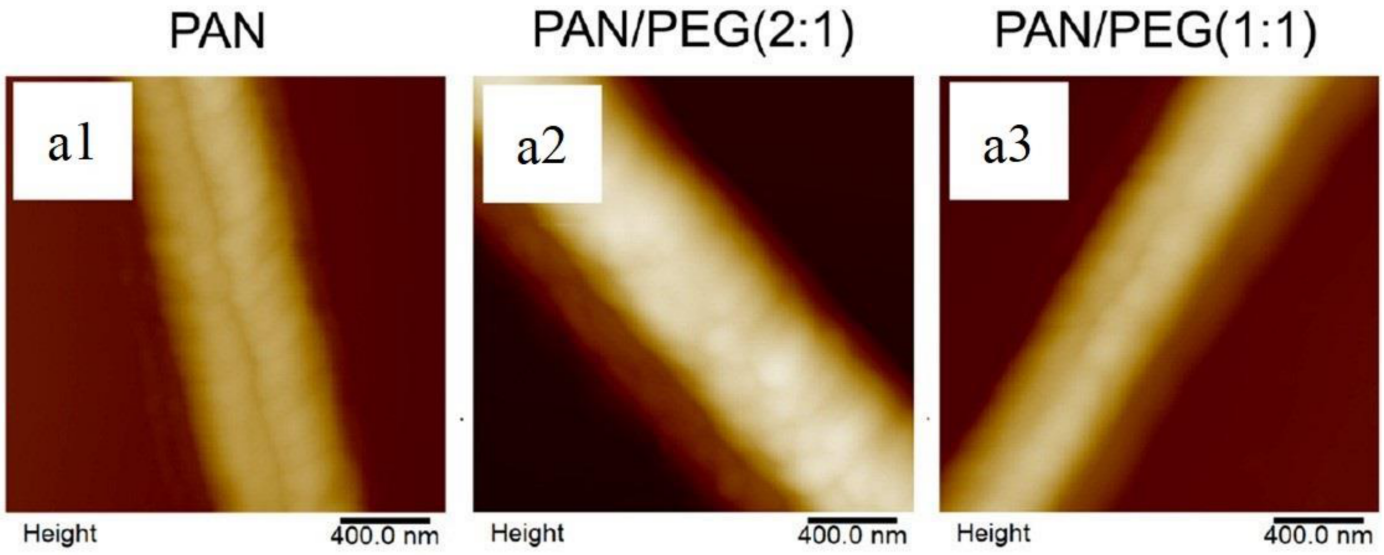

(**a**)

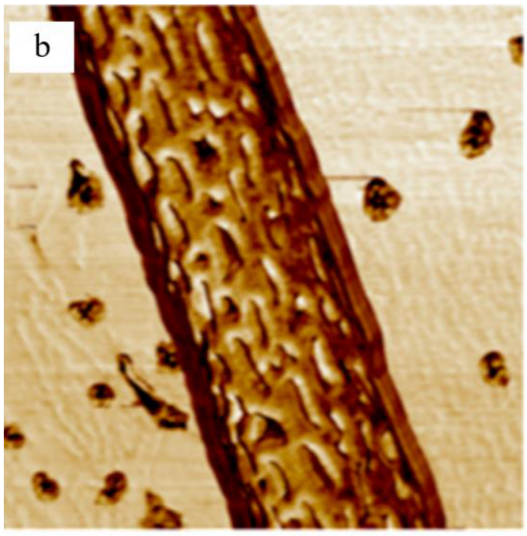

(**b**)

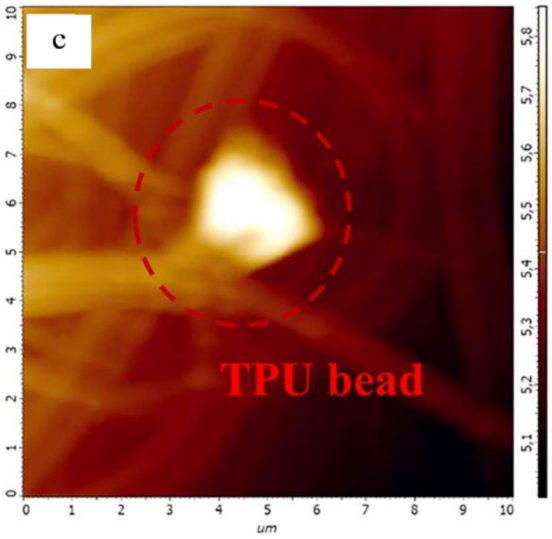

(**c**)

Figure 4. Atomic force microscopy (AFM) images of nanofibers. (**a**) PAN and PAN/poly(ethylene glycol) (PEG) fibers with different blend ratios, reprinted with permission from [68], Copyright, 2022, Elsevier; (**b**) AFM phase image of a poly (L-lactic acid) (PLLA) nanofiber, reproduced from [69], originally published under a CC-BY license; (**c**) topography of polyethylene terephthalate/thermoplastic polyurethane (PET/TPU) nanofiber with TPU bead, reprinted from [70], originally published under a CC-BY license.

While such morphological investigations of single or few nanofibers can often be found in the literature, there are other AFM modes that can be used to measure more properties of nanofiber than just pure morphology, as described in the next section.

4. Other AFM Techniques to Investigate Single Nanofibers

Atomic force microscopy can not only be used to measure surface topography but also to detect several more properties depending on the chosen modes and cantilevers, which are briefly described here.

Magnetic properties, e.g., can be measured with high spatial resolution by magnetic force microscopy (MFM) [71,72]. MFM measurements can be performed relatively simply on flat surfaces, using a special cantilever with a magnetized tip and applying a specific double-scanning technique to separate morphological from magnetic information. On nanofiber mats, however, MFM measurements are much more complicated due to the great height differences and large pores between neighboring nanofibers [73]. Only a few experimental reports of MFM on electrospun nanofiber mats can thus be found in the literature [74,75]. Interestingly, more studies have used MFM on single nanofibers or nanowires placed on a sample holder, reducing the problem of height differences [73]. Nevertheless, the interpretation of the magnetic configuration in such nanowires or nanofibers is not straightforward and needs proper interpretation [76–78]. Especially the stray field of the tip may influence the measurement results and make their interpretation complicated [79], leading to studies that verified their finding by micromagnetic simulations [80] or even developed new MFM tips to tailor the stray fields [81].

Kelvin probe force microscopy (KPFM) can be used to measure the surface potential (or work function) on a wide variety of materials using a conductive AFM tip [82]. Measuring the force between the sample and tip is possible in the amplitude modulation mode, i.e., the intermediate mode in which the cantilever oscillates near its resonance frequency, while the force gradient is measured in the frequency modulation mode, i.e., the non-contact mode [82]. Using this technique, Wu et al. measured the photocatalytic performance of single TiO_2 nanofibers under illumination [83]. Measuring the surface potential of self-assembled poly(3-hexylthiophene) (P3HT) nanofibers by KPFM, Liscio et al. mentioned the necessity to simulate the KPFM image in order to extract the surface potential of very fine nanofibers from KPFM measurements [84]. Deconvolution procedures to increase the resolution of KPFM were also investigated in other studies [85]. However, KPFM measurements on nanofiber mats or single nanofibers are not often reported in the literature.

Piezoresponse force microscopy (PFM) can be used to measure the local piezoelectric deformation of a specimen due to the electric field applied by the AFM tip, enabling making ferroelectric domains visible [86]. This technique was used, e.g., to measure the out-of-plane and in-plane piezoelectric response of poly(vinylidene fluoride) (PVDF) nanofibers [87]. On $Pb(Zr_{0.52}Ti_{0.48})O_3$-$CoFe_2O_4$ composite nanofibers, PFM was used to map Young's modulus on multiferroic nanofibers [88]. An improved so-called dual-frequency resonance tracking PFM technique was applied to map ferroelectric domains in a $BiFeO_3$ nanofiber with very small out-of-plane piezoresponse [89]. PFM measurements on different PVDF/Fe_3O_4 nanofibers revealed differences between the single nanofibers, while the results along one single nanofiber were similar [90].

Scanning thermal microscopy (SThM) can be used to measure thermal conductivity on the nanoscale [91]. Besides a special SThM probe, which is thermally active or thermally sensitive, using a nanoscale thermocouple or resistor, the instrument needs a high temporal resolution with milli- to microseconds thermal time constant to enable these measurements [92]. Only a few studies of SThM on nanofibers can be found in the literature, e.g., measuring the thermal performance of polyimide (PI) nanofibers with thermally conductive silicon nitride (SiN) nanoparticles [93], thermoplastic polyurethane fibers with SiN nanoparticles [94], or carbon/boron nitride nanotubes [95].

Finally, the PeakForce quantitative nanomechanical mapping (PFQNM) mode available in some AFMs should be mentioned, which allows for measuring Young's modulus of different materials [96]. This technique is often applied to cells and in other biophysical investigations [97,98]. Only a few studies on single nanofibers can be found in the literature, such as PFQNM on differently functionalized cellulose nanofibers [99] or on modified chitosan nanofibers [100].

5. Conductivity Measurements of Single Nanofibers

Measuring the electric conductivity of a nanofiber mat is not easy, as the Ohm meter/multimeter or impedance spectrum analyzer, used for DC or AC conductivity measurements, respectively, needs good contact with the conductive nanofiber mat without destroying the nanofibrous structure [101,102]. Contacting a single nanofiber electrically, however, requires much more preparation.

One possibility to prepare a four-probe measurement setup for single nanofibers was described by Wang et al. [103]. Starting with a Si/SiO_2 substrate, they deposited a patterned Au film (Figure 5a), etched the area between the electrodes away (Figure 5b), positioned the nanofiber for measurement (Figure 5c), bonded it by the conductive ionomer, which also formed the nanofiber (Figure 5d), and finally performed four-probe impedance measurements (Figure 5e). By this technique, they could show the negative influence of the carrier polymer PEO on the proton conductivity of a Nafion/PEO nanofiber as well as the high sensitivity of this nanofiber on the relative humidity, while the proton conductivity of a nanofiber with diameter 650 nm at 25 °C and 97% relative humidity was approximately 10^{-2} S/cm [103].

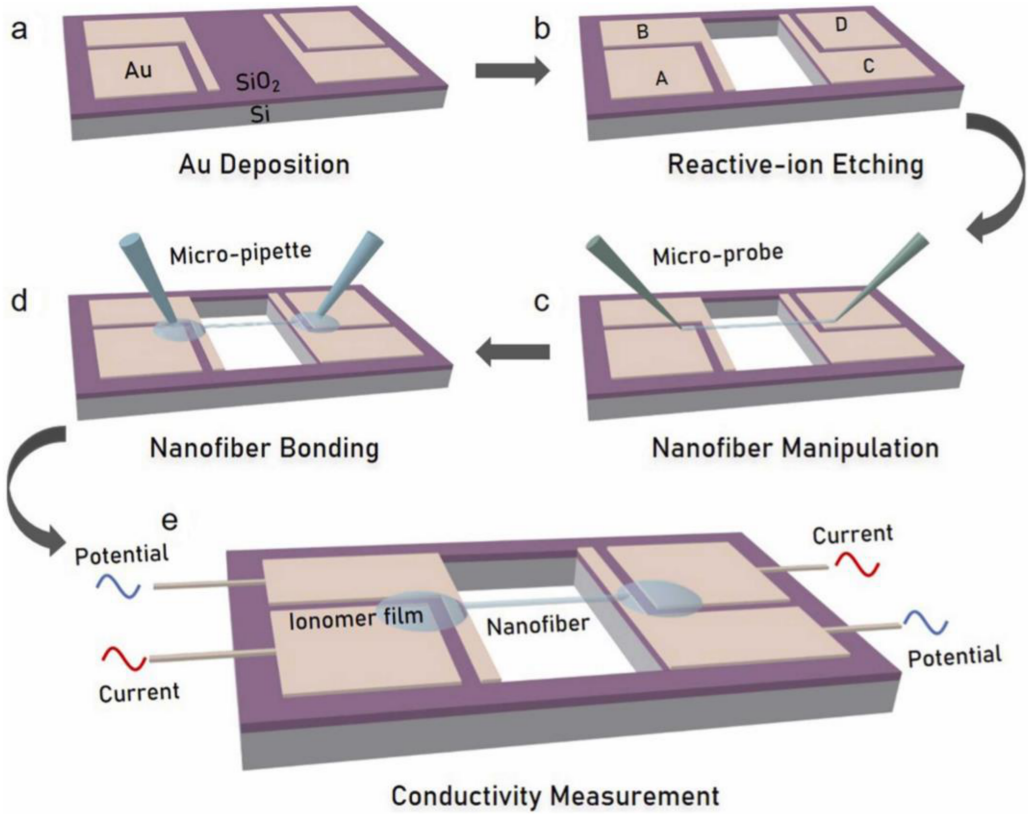

Figure 5. Preparation process of a micro-electrode with ionomer nanofiber. (**a**) Deposit Au on the silicon substrate with an oxide layer on the surface; (**b**) Etch the substrate between the middle electrodes by Reactive-Ion Etching (RIE) method. (**c**) Place the nanofiber on the micro-electrode by micro-probe using the nanofiber manipulation system; (**d**) Inject tiny droplets of ionomer solution to the contact region between nanofiber and micro-electrode by micro-pipette; (**e**) Dry the ionomer droplets into film and conduct impedance measurement. Electrode A and D are the current-carrying electrodes, and electrodes B and C are the potential-sensing electrodes in the four-probe setup. Reprinted with permission from [103], Copyright 2022, Elsevier.

In a similar way, Sengupta et al. measured the conductivity of single carbonized PAN nanofibers by direct electrospinning them on micro-trench substrates positioned on a fast-rotating cylindrical collector, resulting in automatic alignment of single fibers across the trench so that measurements could be performed by connecting the conducting electrodes

between the nanofiber was located by glued Cu strips, as depicted in Figure 6 [104]. A similar method was suggested by Mondal et al. to measure Ag/C nanofibers [105].

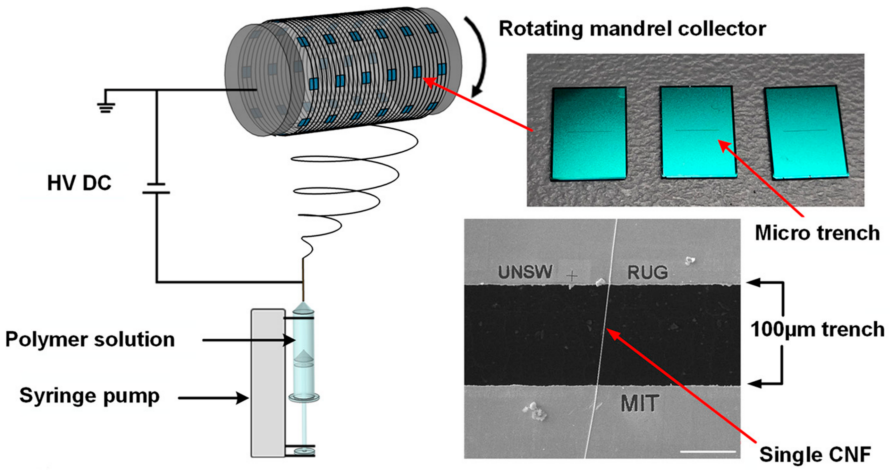

Figure 6. Schematic of the electrospinning setup for single PAN nanofibers across micro-trench and nanofiber bundles on an aluminum foil substrate; photograph of the fabricated micro-trench sample; SEM image of electrospun single PAN nanofibers across the micro-trench. Reprinted from [104], originally published under a CC-BY license.

Placing a conductive nanofiber over the 40 μm broad gap between two electrodes and measuring current-voltage curves was also used by Serrano-Garcia et al. to measure the conductivity of single poly(3-hexylthiophene-2,5-diyl)/polystyrenepoly(benzimidazobenzophenanthroline) (P3HT/PS-BBL) nanofibers with P3HT/PS core and BBL shell, detecting a conductivity around 1.4×10^{-4} S/m [106]. Similarly, Lee et al. deposited a single conductive nanofiber over an array of gold contacts with distances 50 μm between them and measured current-voltage curves to receive the Ohmic resistance of around 1.6 kS/m [107].

Another way to establish a four-probe contact with a single titanium oxynitride (TiO_xN_y) carbon composite nanofiber was described by Koderman Podborsek et al., who connected the four measurement chip's contacts with the nanofiber by platinum deposited by focused ion-beam (FIB), resulting in conductivity values around 1 kS/m [108]. In a similar way, Henrichsen et al. contacted single nanofibers by placing them on silicon dioxide support and coating electrodes, separated by a shadow mask to receive two unconnected conductive electrode areas, as shown in Figure 7 [109].

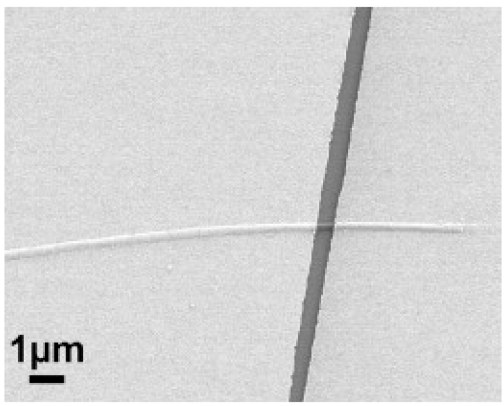

Figure 7. SEM image of a conductive nanofiber on a silicon dioxide support with electrodes separated by the shadow of a silicon wire mask. Reprinted with permission from [109], Copyright 2007, Elsevier.

An interesting test was performed by Qi et al., who measured the conductivity of nanofibers along the fiber direction and perpendicular to it [110]. For this, they prepared

samples with aligned nanofibers and measured parallel and perpendicular to the fiber direction by covering parts of the nanofiber mats with thin conductive sheets, as shown in Figure 8, resulting in conductivities in the range of 10^{-6}–10^{-3} S in the conductive direction and of around 10^{-10} S in the insulating direction [110]. It should be mentioned that this measurement method is not related to single fibers but is added here as an example of how conductivity perpendicular to the fiber direction may be made measurable.

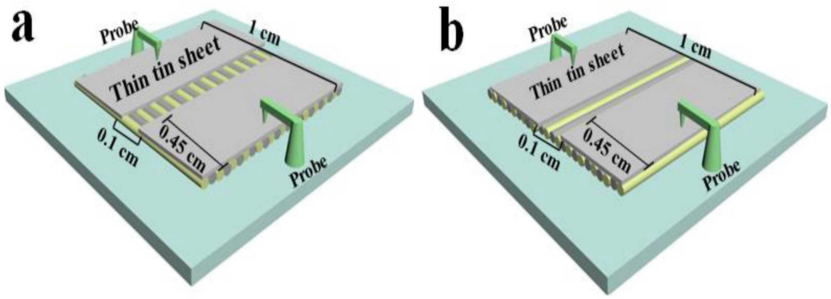

Figure 8. Test method for the conductive anisotropy of the samples. (**a**) Measuring conductivity along the fibers; (**b**) measuring conductivity perpendicular to the fibers. Reprinted from [110], with permission from Elsevier.

6. Measuring the Wettability of Single Nanofibers

Due to the importance of wettability in diverse applications, this parameter is often measured on nanofiber mats [24,25]. For such nanofibrous membranes, the wettability can not only be modified by the material composition of the nanofibers [66,111,112] and a potential chemical or thermal post-treatment [113,114], but it also depends on the nanofiber diameters [115]. The wettability of nanofiber mats is mostly related to the water contact angle (or contact angle measured for other fluids that are relevant for a specific application) [116–118], but water uptake and drying rate are sometimes also taken into account in the definition of wettability [115].

For single nanofibers, water uptake and drying rate are not well-defined. The water contact angle, on the other hand, can not easily be measured on a single nanofiber, as a droplet for the sessile drop test—the most common method to measure the water contact angle [119–121]—would have to be smaller than the nanofiber diameter. While wetting inside nanotubes and nanochannels is indeed studied in theory and experiment [122], experimental investigations of sessile nanodrops on nanofibers are usually not found in the literature. Besides experimental challenges, this may also be attributed to the wetting properties of nanofibers differing from those of plain solid surfaces [123].

Interestingly, measuring the contact angle is nevertheless possible on single nanofibers. For this, the so-called Wilhelmy force balance method is used [124,125]. Its principle is depicted in Figure 9 [126]. For such measurements, a nanofiber is usually attached to the tip of an AFM by a nanomanipulator and fixed by a drop of glue so that it can be inserted into a probe liquid, and the force (in the range of nN) due to the fiber-liquid contact is measured [127]. This force is equal to $F = \gamma d cos\theta$ with the surface tension γ of the liquid, the nanofiber diameter d, and the liquid-nanofiber wetting contact angle θ, which is the only unknown parameter [127].

Some studies have reported single nanofiber contact angles based on this technique. Wang et al. used it to measure the contact angle on carbon fibers with grafted carbon nanofibers [128], while Barber et al. examined single carbon nanotubes [124,129]. Stachewicz et al. measured contact angles on PA6 nanofibers [130] and examined wetting differences between complete nanofiber mats and single nanofibers [131]. Yazdanpanah et al. used metal alloy nanowires instead, grown on the AFM probe, to investigate the contact angle with different low molecular weight liquids [132].

However, in spite of the available and well-known technique, the number of studies of single nanofiber wetting behavior is still small. This is different for measurements of

the mechanical properties of single nanofibers, although the measurement techniques are similarly complicated, as shown in the next section.

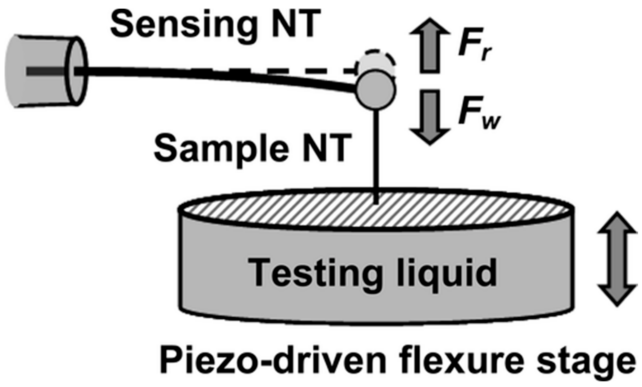

Figure 9. Wilhelmy force balance method, showing nanotubes NT for testing and as a sample introduced in a test liquid. Reprinted with permission from [126]. Copyright 2006, American Chemical Society.

7. Measuring the Mechanical Properties of Single Nanofibers

Among the typical mechanical properties that can be measured on macroscopic scales, mechanical stability, and flexibility are amongst the most important ones for nanofiber mats used in energy applications [28]. This is especially important for carbonized nanofiber mats in which mechanical robustness and foldability are often reduced as compared to as-spun polymeric nanofiber mats, strongly depending on stabilization and carbonization parameters as well as nanofiber orientation, spinning parameters, and spinning solution [133–135].

For single nanofibers, measuring different mechanical properties typically involves an atomic force microscope. Tan et al. described a tensile test on a single PEO nanofiber [136]. They used an inverted microscope stage to stretch the nanofiber, which was glued on a coverslip, and a piezoresistive AFM cantilever with a known spring constant to measure the tensile load. Nanofiber manipulation was performed by so-called femtotips, i.e., ultrafine-tipped micropipettes. Electrospinning was performed for a short time using a wooden frame with parallel conductive strings as a substrate to gain single nanofibers, which leads to highly aligned nanofibers oriented perpendicular to the conductive strings. In this way, stress-strain curves of single PEO nanofibers could be measured, resulting in Young's modulus of approximately 45 MPa [136]. In a similar way, Zou et al. investigated the influence of pre-oxidation on the mechanical properties of single PAN nanofibers and found the highest strength, modulus, and toughness for a pre-oxidation temperature of 210 °C [137].

A similar approach was used by Hwang et al., who performed tensile tests with an AFM cantilever inside a scanning electron microscope [138]. Here, both ends of a PA 6 nanofiber are fixed, and the cantilever hooks the nanofiber (Figure 10a), elongates it (Figure 10b), and drags it further (Figure 10c) until it breaks (Figure 10d). The authors mentioned using a cantilever with a conical tip instead of a pyramidal one to avoid fiber fracture at the contact point. In this way, they found maximum elongations of 44–130% as well as a tensile strength of 364–94 MPa for nanofibers with diameters of 60–170 nm [138]. The idea of fixing both ends of a nanofiber and dragging it apart by an AFM tip in the middle was also used by Alharbi et al., who investigated PCL nanofibers in this way and found Young's modulus to decrease from 3 GPa to 0.5 GPa upon increasing the nanofiber diameter from 40 nm to 100 nm [139]. Similarly, Sharpe et al. measured fibrinogen:PCL nanofibers, where they found strong strain softening from 1.1 GPa (for 5–10% strain) to 110 MPa (for more than 40% strain) [140], while Baker et al. reported a tensile modulus of around 62 MPa for single PCL nanofibers [141].

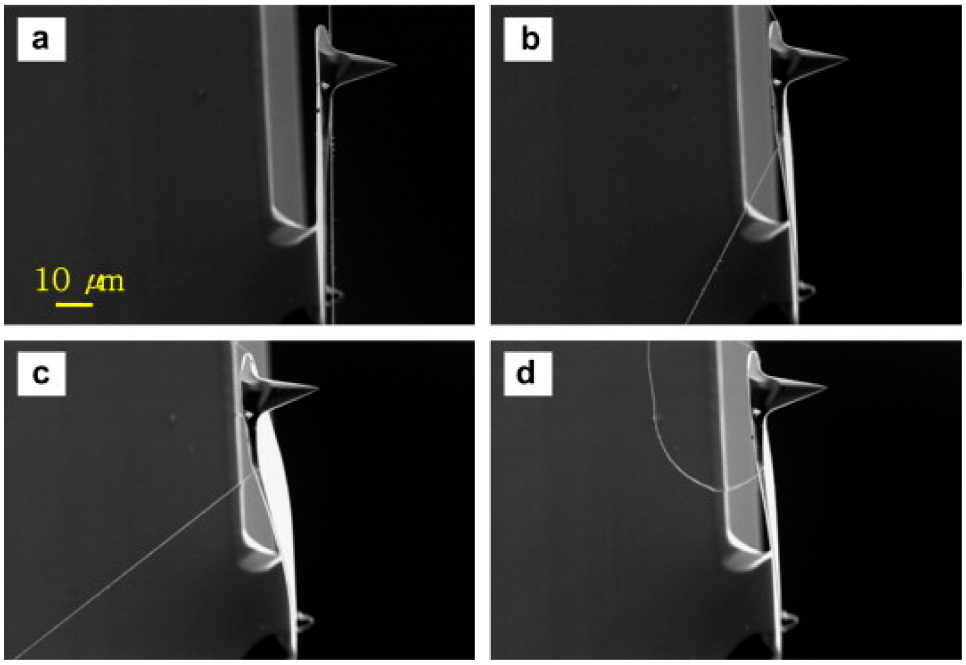

Figure 10. The procedure of the nano-tensile test: (**a**) fiber hook-up, (**b**) fiber elongation, (**c**) further fiber elongation, and (**d**) fiber fracture and entanglement. Reprinted with permission from [138], Copyright 2010, Elsevier.

Another mechanical investigation of nanofibers was suggested by Parvej et al., who examined the transverse elastic modulus of cellulose nanofibrils using AFM-based nanoindentation on top of the nanofiber surface [142]. By measuring normal force vs. z-piezo displacement on top of the cellulose nanofibril in comparison with the normal force for the same measurement on the silicon wafer below, they modeled the elastic modulus from different analytical models and assumptions, resulting in a transverse elastic modulus of (6.9 $\pm$ 0.4) GPa [142]. Nanoindentation by an AFM tip was also used by Bidhar et al. to calculate Young's modulus of zirconia nanofibers from force-distance measurements by some assumptions and models, leading to a value of around 190 GPa [143]. Similarly, Bulbul et al. calculated Young's modulus of single biocomposite nanofibers by nanoindentation [144].

In a more complex setup, Cheng and Wang mounted a cellulose nanofibril over a groove with defined length and measured the deflection of the fibril at this position (Figure 11) [145]. By also measuring the cantilever deflection on the waiver and on the cellulose fibril where it is placed on the waver, they could evaluate the difference between the values measured at these different positions to differentiate deflection from compression of the fibril. The elastic modulus, calculated by beam theory for a long beam with both ends fixed, was found to be approx. 93 GPa for a cellulose nanofibril of diameter 170 nm [145].

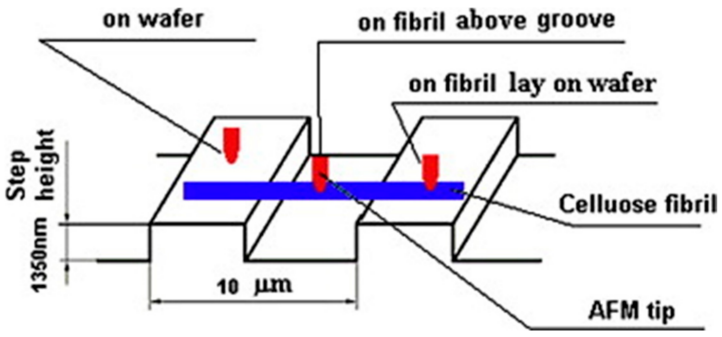

Figure 11. Three AFM tip testing positions during the bending test. Reprinted with permission from [145], Copyright 2008, Elsevier.

As mentioned before, calculations of mechanical properties from nanoindentation, nano-tensile, and nano-bending tests are not easy and necessitate several models and assumptions. An overview of such calculations of the mechanical properties from different AFM-based mechanical test methods for single nanofibers or nanowires can be found in Ref. [146].

8. Other Microscopic Techniques to Investigate Single Nanofibers

Besides the aforementioned techniques to investigate different parameters of nanofibers, a few more should be mentioned here. Scanning near-field optical microscopy (SNOM) can be used to measure the propagation of excited surface plasmon polaritons in nanofibrous waveguides [147] for nanoscale morpho-chemical profiling of polymer blend nanofibers [148] or detection of the molecular orientation angles in nanofibers [149]. Polarized (confocal) Raman microscopy enables quantifying molecular orientation and crystal structure of single nanofibers [150,151] or characterization of the chemical structure and morphology of core-shell nanofibers [152]. Tip-enhanced Raman scattering (TERS) allows for detecting water-decorated carboxyl/hydroxyl groups at edge atoms of carbon-coated fibers [153] or measuring spectral modes of carbon nanotubes [154].

The properties of single nanofibers described in this section are different from the previously defined most important properties of nanofibers for energy applications (as defined at the end of Section 2) and are thus not described in more detail.

9. Conclusions

This review gives an overview of measurements on single nanofibers, concentrating on the physical values most important for energy applications, i.e., porosity and surface roughness, conductivity, wettability, and mechanical properties. Most of these parameters can be measured using AFM-based techniques. In the cited papers, usually, only a few single nanofibers are investigated due to the great effort necessary for single nanofiber contacting/fixation and performing the planned measurements. Nevertheless, we hope that this overview will inspire more authors to use these techniques, especially since an AFM is available in many research groups, to gain more precise measurements instead of the common values averaged over parts of nanofiber mats.

Author Contributions: Conceptualization, A.E. and T.B.; formal analysis, T.B., N.S.M. and A.E.; investigation, N.S.M.; writing—original draft preparation, A.E.; writing—review and editing, T.B. and N.S.M.; visualization, N.S.M. All authors have read and agreed to the published version of the manuscript.

Funding: The article was written during a research stay of Nonsikelelo Sheron Mpofu at Bielefeld University of Applied Sciences and Arts (HSBI). The research stay was funded through the New Horizons Fellowship from HSBI's Central Gender and Diversity Officer.

Data Availability Statement: No new data were created or analyzed in this study. Data sharing is not applicable.

Conflicts of Interest: The authors declare no conflicts of interest. The funders had no role in the design of the study; in the collection, analyses, or interpretation of data; in the writing of the manuscript; or in the decision to publish the results.

References

1. Wang, Z.Q.; Wu, S.S.; Wang, J.; Yu, A.; Wei, G. Carbon nanofiber-based functional nanomaterials for sensor applications. *Nanomaterials* **2019**, *9*, 1045. [CrossRef] [PubMed]
2. Koo, W.-T.; Choi, S.-J.; Kim, N.-H.; Jang, J.-S.; Kim, I.-D. Catalyst-decorated hollow WO_3 nanotubes using layer-by-layer self-assembly on polymeric nanofiber templates and their application in exhaled breath sensor. *Sens. Act. B Chem.* **2016**, *223*, 301–310. [CrossRef]
3. Wang, Q.N.; Yildiz, O.; Li, A.; Aly, K.; Qiu, Y.P.; Jiang, Q.R.; Pui, D.Y.H.; Chen, S.-C.; Bradford, P.D. High temperature carbon nanotube—Nanofiber hybrid filters. *Sep. Purif. Technol.* **2020**, *236*, 116255. [CrossRef]

4. Yalcinkaya, F. A review on advanced nanofiber technology for membrane distillation. *J. Eng. Fibers Fabr.* **2019**, *14*, 1558925018824901. [CrossRef]
5. Grothe, T.; Böhm, T.; Habashy, K.; Abdullaeva, O.S.; Zablocki, J.; Lützen, A.; Dedek, K.; Schiek, M.; Ehrmann, A. Optical index matching, flexible electrospun substrates for seamless organic photocapacitive sensors. *Phys. Stat. Sol. B* **2021**, *258*, 2170021. [CrossRef]
6. Sakamoto, H.; Fujiwara, I.; Takamura, E.; Suye, S.-i. Nanofiber-guided orientation of electrospun carbon nanotubes and fabrication of aligned CNT electrodes for biodevice applications. *Mater. Chem. Phys.* **2020**, *245*, 122745. [CrossRef]
7. Kim, Y.Y.; Le, T.-H.; Kim, S.; Park, G.S.; Yang, K.S.; Yoon, H.S. Single-walled carbon nanotube-in-binary-polymer nanofiber structures and their use as carbon precursors for electrochemical applications. *J. Phys. Chem. C* **2018**, *122*, 4189–4198. [CrossRef]
8. Banitaba, S.N.; Ehrmann, A. Application of electrospun nanofibers for fabrication of versatile and highly efficient electrochemical devices: A review. *Polymers* **2021**, *13*, 1741. [CrossRef]
9. Prabu, G.T.V.; Dhurai, B. A novel profiled multi-pin electrospinning system for nanofiber production and encapsulation of nanoparticles into nanofibers. *Sci. Rep.* **2020**, *10*, 4302. [CrossRef]
10. Ibrahim, H.M.; Klingner, A. A review on electrospun polymeric nanofibers: Production parameters and potential applications. *Polym. Test.* **2020**, *90*, 106647. [CrossRef]
11. Toriello, M.; Afsari, M.; Shon, H.K.; Tijing, L.D. Progress on the fabrication and application of electrospun nanofiber composites. *Membranes* **2020**, *10*, 204. [CrossRef] [PubMed]
12. Moulefera, I.; Trabelsi, M.; Mamun, A.; Sabantina, L. Electrospun carbon nanofibers from biomass and biomass blends—Current trends. *Polymers* **2021**, *13*, 1071. [CrossRef] [PubMed]
13. Yadav, D.; Amini, F.; Ehrmann, A. Recent advances in carbon nanofibers and their applications—A review. *Eur. Polym. J.* **2020**, *138*, 109963. [CrossRef]
14. Mamun, A.; Kiari, M.; Sabantina, L. A recent review of electrospun porous carbon nanofiber mats for energy storage and generation applications. *Membranes* **2023**, *13*, 830. [CrossRef]
15. Surovcík, J.; Medvecká, V.; Gregus, J.; Gregor, M.; Roch, T.; Annusová, A.; Durina, P.; Vojteková, T. Characterization of TiO_2 nanofibers with enhanced photocatalytic properties prepared by plasma assisted calcination. *Ceram. Int.* **2022**, *48*, 37322–37332. [CrossRef]
16. Khalili, S.; Chenari, H.M. Successful electrospinning fabrication of ZrO_2 nanofibers: A detailed physical—Chemical characterization study. *J. Alloys Comp.* **2020**, *828*, 154414. [CrossRef]
17. Blachowicz, T.; Ehrmann, A. Recent developments in electrospun ZnO nanofibers: A short review. *J. Eng. Fibers Fabr.* **2020**, *15*, 1558925019899682. [CrossRef]
18. Liu, X.Y.; Jiang, Y.; Song, X.P.; Qin, C.R.; Wang, S.F.; Li, K.C. A bio-mechanical process for cellulose nanofiber production—Towards a greener and energy conservation solution. *Carbohydr. Polym.* **2019**, *208*, 191–199. [CrossRef]
19. Sánchez-Gutiérrez, M.; Espinosa, E.; Bascón-Villegas, I.; Pérez-Rodríguez, F.; Carrasco, E.; Rodríguez, A. Production of cellulose nanofibers from olive tree harvest—A residue with wide applications. *Agronomy* **2020**, *10*, 696. [CrossRef]
20. Fahmi Supian, M.A.; Mohd Amin, K.N.; Jamari, S.S.; Mohamad, S. Production of cellulose nanofiber (CNF) from empty fruit bunch (EFB) via mechanical method. *J. Environ. Chem. Eng.* **2020**, *8*, 103024.
21. Zhou, X.X.; Liu, B.; Chen, Y.; Guo, L.; Wei, G. Carbon nanofiber-based three-dimensional nanomaterials for energy and environmental applications. *Mater. Adv.* **2020**, *1*, 2163–2181. [CrossRef]
22. Joshi, J.S.; Langwald, S.V.; Ehrmann, A.; Sabantina, L. Algal-based biopolymers for batteries and biofuel application in comparison with bacterial biopolymers—A review. *Polymers* **2024**, *16*, 610. [CrossRef] [PubMed]
23. Khademolqorani, S.; Banitaba, S.N.; Gupta, A.; Poursharifi, N.; Ghaffari, A.A.; Jadhav, V.V.; Ul Arifeen, W.; Sing, M.; Borah, M.; Chamanehpour, E.; et al. Application scopes of miniaturized MXene-functionalized electrospun nanofibers-based electrochemical energy devices. *Small* **2024**, *20*, 2309572. [CrossRef]
24. Dahal, B.; Mukhiya, T.; Ojha, G.P.; Muthurasu, A.; Chae, S.H.; Kim, T.; Kang, D.W.; Kim, H.Y. In-built fabrication of MOF assimilated B/N co-doped 3D porous carbon nanofiber network as a binder-free electrode for supercapacitors. *Electrochim. Acta* **2019**, *301*, 209–219. [CrossRef]
25. Lei, W.; Zhang, H.J.; Liu, D.Z.; Lin, L.X. Fabrication of nitrogen and sulfur co-doped carbon nanofibers with three-dimensional architecture for high performance supercapacitors. *Appl. Surf. Sci.* **2019**, *495*, 143572. [CrossRef]
26. Liu, Y.W.; Liu, Q.; Wang, L.; Yang, X.F.; Yang, W.Y.; Zheng, J.J.; Hou, H.L. Advanced supercapacitors based on porous hollow carbon nanofiber electrodes with high specific capacitance and large energy density. *ACS Appl. Mater. Interfaces* **2020**, *12*, 4777–4786. [CrossRef]
27. Lin, C.H.; Tsai, C.H.; Tseng, F.G.; Chen, I.C.; Hsieh, C.K. Electrochemical pulse deposition of Ni nanoparticles on the 3D graphene network to synthesize vertical CNFs as the full-carbon hybrid nanoarchitecture for supercapacitors. *Mater. Lett.* **2017**, *192*, 40–43. [CrossRef]
28. Nie, G.D.; Zhao, X.W.; Luan, Y.X.; Jiang, J.M.; Kou, Z.K.; Wang, J. Key issues facing electrospun carbon nanofibers in energy applications: On-going approaches and challenges. *Nanoscale* **2020**, *12*, 13225–13248. [CrossRef] [PubMed]
29. Massaglia, G.; Margaria, V.; Sacco, A.; Castellino, M.; Chiodoni, A.; Pirri, F.C.; Quaglio, M. N-doped carbon nanofibers as catalyst layer at cathode in single chamber microbial fuel cells. *Int. J. Hydrog. Energy* **2019**, *44*, 4442–4449. [CrossRef]

30. Shi, Q.; Wang, Y.D.; Wang, Z.M.; Lei, Y.P.; Wang, B.; Wu, N.; Han, C.; Gou, Y.Z. Three-dimensional (3D) interconnected networks fabricated via in-situ growth of N-doped graphene/carbon nanotubes on Co-containing carbon nanofibers for enhanced oxygen reduction. *Nano Res.* **2016**, *9*, 317–328. [CrossRef]
31. Liu, Y.X.; Si, L.; Du, Y.C.; Zhou, X.S.; Dai, Z.H.; Bao, J.C. Strongly bonded selenium/microporous carbon nanofibers composite as a high-performance cathode for lithium-selenium batteries. *J. Phys. Chem. C* **2015**, *119*, 27316–27321. [CrossRef]
32. Wang, M.; Yang, Y.; Yang, Z.Z.; Gu, L.; Chen, Q.W.; Yu, Y. Sodium-ion batteries: Improving the rate capability of 3D interconnected carbon nanofibers thin film by boron, nitrogen dual-doping. *Adv. Sci.* **2017**, *4*, 1600468. [CrossRef] [PubMed]
33. Feng, M.J.; Chi, Q.G.; Feng, Y.; Zhang, Y.; Zhang, T.D.; Zhang, C.H.; Chen, Q.G.; Lei, Q.Q. High energy storage density and efficiency in aligned nanofiber filled nanocomposites with multilayer structure. *Compos. B Eng.* **2020**, *198*, 108206. [CrossRef]
34. Yan, Y.H.; Liu, X.Y.; Yan, J.; Guan, C.; Wang, J. Electrospun nanofibers for new generation flexible energy storage. *Energy Environ. Mater.* **2021**, *4*, 502–521. [CrossRef]
35. Gu, H.H.; Huang, Y.P.; Zuo, L.Z.; Fan, W.; Liu, T.X. Graphene sheets wrapped carbon nanofibers as a highly conductive three-dimensional framework for perpendicularly anchoring of MoS_2: Advanced electrocatalysts for hydrogen evolution reaction. *Electrochim. Acta* **2016**, *219*, 604–613. [CrossRef]
36. Shao, Y.; Luo, C.; Deng, B.-w.; Yin, B.; Yang, M.-b. Flexible porous silicone rubber-nanofiber nanocomposites generated by supercritical carbon dioxide foaming for harvesting mechanical energy. *Nano Energy* **2020**, *67*, 104290. [CrossRef]
37. Shi, L.; Jin, H.; Dong, S.R.; Huang, S.Y.; Kuang, H.Z.; Xu, H.S.; Chen, J.K.; Xuan, W.P.; Zhang, S.M.; Li, S.J.; et al. High-performance triboelectric nanogenerator based on electrospun PVDF-graphene nanosheet composite nanofibers for energy harvesting. *Nano Energy* **2021**, *80*, 105599. [CrossRef]
38. Guan, X.Y.; Xu, B.G.; Wu, M.J.; Jing, T.T.; Yang, Y.J.; Gao, Y.Y. Breathable, washable and wearable woven-structured triboelectric nanogenerators utilizing electrospun nanofibers for biomechanical energy harvesting and self-powered sensing. *Nano Energy* **2021**, *80*, 105549. [CrossRef]
39. Babu, A.; Aazem, I.; Walden, R.; Bairagi, S.; Mulvihill, D.M.; Pillai, S.C. Electrospun nanofiber based TENGs for wearable electronics and self-powered sensing. *Chem. Eng. J.* **2023**, *452*, 139060. [CrossRef]
40. Jiang, F.; Zhou, X.R.; Lv, J.; Chen, J.; Chen, J.T.; Kongcharoen, H.; Zhang, Y.H.; Lee, P.S. Stretchable, breathable, and stable lead-free perovskite/polymer nanofiber composite for hybrid triboelectric and piezoelectric energy harvesting. *Adv. Mater.* **2022**, *34*, 2200042. [CrossRef]
41. He, X.Y.; Gu, J.T.; Hao, Y.N.; Zheng, M.R.; Wang, L.M.; Yu, J.Y.; Qin, Q.H. Continuous manufacture of stretchable and integratable thermoelectric nanofiber yarn for human body energy harvesting and self-powered motion detection. *Chem. Eng. J.* **2022**, *450*, 137937. [CrossRef]
42. Xie, L.; Zhou, S.; Liu, J.R.; Qiu, B.L.; Liu, T.Y.; Liang, Q.R.; Zheng, X.Z.; Li, B.; Zeng, J.; Yan, M.; et al. Sequential superassembly of nanofiber arrays to carbonaceous ordered mesoporous nanowires and their heterostructure membranes for osmotic energy conversion. *J. Am. Chem. Soc.* **2021**, *143*, 6922–6932. [CrossRef] [PubMed]
43. Wu, Y.D.; Xin, W.W.; Kong, X.-Y.; Chen, J.J.; Qian, Y.C.; Sun, Y.; Zhao, X.L.; Chen, W.P.; Jiang, L.; Wen, L.P. Enhanced ion transport by graphene oxide/cellulose nanofibers assembled membranes for high-performance osmotic energy harvesting. *Mater. Horiz.* **2020**, *7*, 2702–2709. [CrossRef]
44. Mamun, A.; Klöcker, M.; Blachowicz, T.; Sabantina, L. Investigation of the morphological structure of needle-free electrospun magnetic nanofiber mats. *Magnetochemistry* **2022**, *8*, 25. [CrossRef]
45. Mamun, A.; Blachowicz, T.; Sabantina, L. Electrospun nanofiber mats for filtering applications—Technology, structure and materials. *Polymers* **2021**, *13*, 1368. [CrossRef] [PubMed]
46. Nishiuchi, H.; Tonami, H. Control of mat thickness in electrospinning with transparent conductive glass collector. *Polym. Eng. Sci.* **2022**, *62*, 2252–2259. [CrossRef]
47. Sharif, N.; Khoshnoudi-Nia, S.; Jafari, S.M. Confocal laser scanning microscopy (CLSM) of nanoencapsulated food ingredients. In *Characterization of Nanoencapsulated Food Ingredients*; Academic Press Elsevier: Amsterdam, The Netherlands, 2020; pp. 131–158.
48. Gallegos-Cerda, S.D.; Hernández-Verela, J.D.; Chanona-Pérez, J.J.; Tamayo, B.A.; Méndez Méndez, J.V. Super-resolution microscopy and their applications in food materials: Beyond the resolution limits of fluorescence microscopy. *Food Bioprocess Technol.* **2022**, *16*, 268–288. [CrossRef]
49. Wortmann, M.; Westphal, M.; Kaltschmidt, B.; Klöcker, M.; Layland, A.S.; Brockhagen, B.; Hütten, A.; Frese, N.; Ehrmann, A. Nanofibers are a matter of perspective: Effects of methodology and subjectivity on diameter measurements. *Nanoscale Adv.* **2023**, *5*, 5900–5906. [CrossRef]
50. Serag, E.; Abd El-Aziz, A.M.; El-Maghraby, A.; Taha, N.A. Electrospun non-wovens potential wound dressing material based on polyacrylonitrile/chicken feathers keratin nanofiber. *Sci. Rep.* **2022**, *12*, 15460. [CrossRef]
51. Rahmani, F.; Ziyadi, H.; Baghali, M.; Luo, H.R.; Ramakrishna, S. Electrospun PVP/PVA nanofiber mat as a novel potential transdermal drug-delivery system for buprenorphine: A solution needed for pain management. *Appl. Sci.* **2021**, *11*, 2779. [CrossRef]
52. Pham Le, Q.; Uspenskaya, M.V.; Olekhnovich, R.O.; Baranov, M.A. The mechanical properties of PVC nanofiber mats obtained by electrospinning. *Fibers* **2021**, *9*, 2. [CrossRef]
53. Vafaye, S.E.; Rahman, A.; Safaeian, S.; Adabi, M. An electrochemical aptasensor based on electrospun carbon nanofiber mat and gold nanoparticles for the sensitive detection of Penicillin in milk. *J. Food Meas. Charact.* **2021**, *15*, 876–882. [CrossRef]

54. Xie, W.H.; Shi, Y.L.; Wang, Y.X.; Zheng, Y.L.; Liu, H.; Hu, Q.; Wie, S.Y.; Gu, H.B.; Guo, Z.H. Electrospun iron/cobalt alloy nanoparticles on carbon nanofibers towards exhaustive electrocatalytic degradation of tetracycline in wastewater. *Chem. Eng. J.* **2021**, *405*, 126585. [CrossRef]
55. Baek, S.H.; Roh, J.H.; Park, C.Y.; Kim, M.W.; Shi, R.J.; Kailasa, S.K.; Park, T.J. Cu-nanoflower decorated gold nanoparticles-graphene oxide nanofiber as electrochemical biosensor for glucose detection. *Mater. Sci. Eng. C* **2020**, *107*, 110273. [CrossRef]
56. Zainab, G.; Babar, A.A.; Ali, N.; Aboalhassan, A.A.; Wang, X.F.; Yu, J.Y.; Ding, B. Electrospun carbon nanofibers with multi-aperture/opening porous hierarchical structure for efficient CO_2 adsorption. *J. Coll. Interface Sci.* **2020**, *561*, 659–667. [CrossRef] [PubMed]
57. Amiri, A.; Conlee, B.; Tallerine, I.; Kennedy, W.J.; Naraghi, M. A novel path towards synthesis of nitrogen-rich porous carbon nanofibers for high performance supercapacitors. *Chem. Eng. J.* **2020**, *399*, 125788. [CrossRef]
58. Saha, D.; Gismondi, P.; Kolasinski, K.W.; Shumlas, S.L.; Rangan, S.; Eslami, B.; McConnell, A.; Bui, T.V.; Cunfer, K. Fabrication of electrospun nanofiber composite of g-C_3N_4 and Au nanoparticles as plasmonic photocatalyst. *Surf. Interfaces* **2021**, *26*, 101367. [CrossRef]
59. Ju, Z.S.; Li, P.; Zhao, X.N.; Ma, J.G.; Xu, H.Y.; Liu, Y.C. Flexible TiN/Co@Carbon nanofiber mats for high-performance electromagnetic interference shielding and Joule heating applications. *Carbon* **2022**, *196*, 612–620. [CrossRef]
60. Mousa, H.M.; Hussein, K.H.; Sayed, M.M.; Abd El-Rahman, M.K.; Woo, H.-M. Development and characterization of cellulose/iron acetate nanofibers for bone tissue engineering applications. *Polymers* **2021**, *13*, 1339. [CrossRef]
61. Wabah, J.A.; Mamun, S.A. Polyacrylonitrile nanofiber mats containing titania/AgNP composite nanoparticles for antibacterial applications. *Mater. Res. Expr.* **2020**, *7*, 015416.
62. Wortmann, M.; Layland, A.S.; Frese, N.; Kahmann, U.; Grothe, T.; Storck, J.L.; Blachowicz, T.; Grzybowski, J.; Hüsgen, B.; Ehrmann, A. On the reliability of highly magnified micrographs for structural analysis in materials science. *Sci. Rep.* **2020**, *10*, 14708. [CrossRef] [PubMed]
63. Yang, J.K.; Wang, K.; Yu, D.-G.; Yang, Y.Y.; Bligh, S.W.A.; Williams, G.R. Electrospun Janus nanofibers loaded with a drug and inorganic nanoparticles as an effective antibacterial wound dressing. *Mater. Sci. Eng. C* **2020**, *111*, 110805. [CrossRef] [PubMed]
64. Wang, Y.L.; Cui, J.X.; Qu, Q.L.; Ma, W.J.; Li, F.H.; Du, W.H.; Liu, K.M.; Zhang, Q.; He, S.J.; Huang, C.B. Free-standing porous carbon nanofiber membranes obtained by one-step carbonization and activation for high-performance supercapacitors. *Microporous Mesoporous Mater.* **2022**, *329*, 111545. [CrossRef]
65. Chlanda, A.; Kijenska-Gawronska, E.; Zdunek, J.; Swieszkowski, W. Internal nanocrystalline structure and stiffness alterations of electrospun polycaprolactone-based mats after six months of *in vitro* degradation. An atomic force microscopy assay. *J. Mech. Behav. Biomed. Mater.* **2020**, *101*, 103437. [CrossRef]
66. Wang, D.; Yue, Y.Y.; Wang, Q.X.; Cheng, W.L.; Han, G.P. Preparation of cellulose acetate-polyacrylonitrile composite nanofibers by multi-fluid mixing electrospinning method: Morphology, wettability, and mechanical properties. *Appl. Surf. Sci.* **2020**, *510*, 145462. [CrossRef]
67. Joshi, J.; Homburg, S.V.; Ehrmann, A. Atomic force microscopy (AFM) on biopolymers and hydrogels for biotechnological applications—Possibilities and limits. *Polymers* **2022**, *14*, 1267. [CrossRef]
68. Liu, X.; Wang, C.M.; Cai, Z.Y.; Hu, Z.J.; Zhu, P. Fabrication and characterization of polyacrylonitrile and polyethylene glycol composite nanofibers by electrospinning. *J. Energy Storage* **2022**, *53*, 105171. [CrossRef]
69. Cuong, N.T.; Barrau, S.; Dufay, M.; Tabary, N.; Da Costa, A.; Ferri, A.; Lazzaroni, R.; Raquez, J.-M.; Leclère, P. On the Nanoscale Mapping of the Mechanical and Piezoelectric Properties of Poly(L-Lactic Acid) Electrospun Nanofibers. *Appl. Sci.* **2020**, *10*, 652. [CrossRef]
70. Guo, Y.H.; Guo, Y.C.; He, W.D.; Zhao, Y.B.; Shen, R.Q.; Liu, J.X.; Wang, J. PET/TPU nanofiber composite filters with high interfacial adhesion strength based on one-step co-electrospinning. *Powder Technol.* **2021**, *387*, 136–145. [CrossRef]
71. Vokoun, D.; Samal, S.; Stachiv, I. Magnetic force microscopy in physics and biomedical applications. *Magnetochemistry* **2022**, *8*, 42. [CrossRef]
72. Winkler, R.; Ciria, M.; Ahmad, M.; Plank, H.; Marcuello, C. A review of the current state of magnetic force microscopy to unravel the magnetic properties of nanomaterials applied in biological systems and future directions for quantum technologies. *Nanomaterials* **2023**, *13*, 2585. [CrossRef]
73. Ehrmann, A.; Blachowicz, T. Magnetic force microscopy on nanofibers—Limits and possible approaches for randomly oriented nanofiber mats. *Magnetochemistry* **2021**, *7*, 143. [CrossRef]
74. Weiss, R.; Ehrmann, A. Preliminary report on MFM measurements on magnetic nanofiber mats. *Commun. Dev. Assem. Text. Prod.* **2021**, *2*, 1–7. [CrossRef]
75. Brocks, O.; Stasiak, A.; Biedinger, J.; Wortmann, M.; Blachowicz, T.; Kaschuba, R.; Ehrmann, A. MOKE and MFM on magnetically coated nanofiber mats: Transferring well-known methods to uncommon samples. *Appl. Res.* **2023**, *2*, e202200113. [CrossRef]
76. Berganza, E.; Jaarar, M.; Bran, C.; Fernández-Roldán, J.A.; Chubykalo-Fesenko, O.; Vázquez, M.; Asenjo, A. Multisegmented nanowires: A step towards the control of the domain wall configuration. *Sci. Rep.* **2017**, *7*, 11576. [CrossRef] [PubMed]
77. Bran, C.; Fernandez-Roldan, J.A.; Palmero, E.M.; Berganza, E.; Guzman, J.; del Real, R.P.; Asenjo, A.; Fraile Rodríguez, A.; Foerster, M.; Aballe, L.; et al. Direct observation of transverse and vortex metastable magnetic domains in cylindrical nanowires. *Phys. Rev. B* **2017**, *96*, 125415. [CrossRef]

78. Askey, J.; Hunt, M.O.; Langbein, W.; Ladak, S. Use of two-photon lithography with a negative resist and processing to realize cylindrical magnetic nanowires. *Nanomaterials* **2020**, *10*, 429. [CrossRef]
79. Nasirpouri, F.; Nogaret, A.; Bending, S.J. Effect of size and configuration on the magnetization of nickel dot arrays. *IEEE Trans. Magn.* **2011**, *47*, 4695–4700. [CrossRef]
80. Nasirpouri, F.; Peighambari-Sattari, S.-M.; Bran, C.; Palmero, E.M.; Berganza Eguiarte, E.; Vazquez, M.; Patsopoulos, A.; Kechrakos, D. Geometrically designed domain wall trap in tri-segmented nickel magnetic nanowires for spintronics devices. *Sci. Rep.* **2019**, *9*, 9010. [CrossRef]
81. Corte-León, H.; Rodríguez, L.A.; Pancaldi, M.; Gatel, C.; Cox, D.; Snoeck, E.; Antonov, V.; Vavassori, P.; Kazakova, O. Magnetic imaging using geometrically constrained nano-domain walls. *Nanoscale* **2019**, *11*, 4478–4488. [CrossRef]
82. Melitz, W.; Shen, J.; Kummel, A.C.; Lee, S.Y. Kelvin probe force microscopy and its application. *Surf. Sci. Rep.* **2011**, *66*, 1–27. [CrossRef]
83. Wu, M.-C.; Liao, H.-C.; Cho, Y.-C.; Tóth, T.; Chen, Y.-F.; Su, W.-F.; Kordás, K. Photo-Kelvin probe force microscopy for photocatalytic performance characterization of single filament of TiO_2 nanofiber photocatalysts. *J. Mater. Chem. A* **2013**, *1*, 5715–5720. [CrossRef]
84. Liscio, A.; Palermo, V.; Samori, P. Probing local surface potential of quasi-one-dimensional systems: A KPFM study of P3HT nanofibers. *Adv. Funct. Mater.* **2008**, *18*, 907–914. [CrossRef]
85. Liscio, A.; Palermo, V.; Samori, P. Nanoscale quantitative measurement of the potential of charged nanostructures by electrostatic and kelvin probe force microscopy: Unraveling electronic processes in complex materials. *Acc. Chem. Res.* **2010**, *43*, 541–550. [CrossRef] [PubMed]
86. Soergel, E. Piezoresponse force microscopy (PFM). *J. Phys. D Appl. Phys.* **2011**, *44*, 464003. [CrossRef]
87. Liu, X.; Kuang, X.L.; Xu, S.X.; Wang, X.H. High-sensitivity piezoresponse force microscopy studies of single polyvinylidene fluoride nanofibers. *Mater. Lett.* **2017**, *191*, 189–192. [CrossRef]
88. Zhu, Q.F.; Pan, K.; Xie, S.H.; Liu, Y.Y.; Li, J.Y. Nanomechanics of multiferroic composite nanofibers via local excitation piezoresponse force microscopy. *J. Mech. Phys. Solids* **2019**, *126*, 76–86. [CrossRef]
89. Xie, S.H.; Gannepalli, A.; Chen, Q.N.; Liu, Y.M.; Zhou, Y.C.; Proksch, R.; Li, J.Y. High resolution quantitative piezoresponse force microscopy of $BiFeO_3$ nanofibers with dramatically enhanced sensitivity. *Nanoscale* **2012**, *4*, 408–413. [CrossRef]
90. Zheng, T.; Yue, Z.L.; Wallace, G.G.; Du, Y.; Martins, P.; Lanceros-Mendez, S.; Higgins, M.J. Local probing of magnetoelectric properties of PVDF/Fe_3O_4 electrospun nanofibers by piezoresponse force microscopy. *Nanotechnology* **2017**, *28*, 065707. [CrossRef]
91. Gomès, S.; Assy, A.; Chapuis, P.-O. Scanning thermal microscopy: A review. *Phys. Stat. Sol. A* **2015**, *212*, 477–494. [CrossRef]
92. Zhang, Y.; Zhu, W.K.; Hui, F.; Lanza, M.; Borca-Tasciuc, T.; Munoz, R. A review on principles and applications of scanning thermal microscopy (SThM). *Adv. Funct. Mater.* **2020**, *30*, 1900892. [CrossRef]
93. Moradi, A.; Szewczyk, P.K.; Stachewicz, U. Bridging a gap in thermal conductivity and heat transfer in hybrid fibers and yarns via polyimide and silicon nitride composites. *Small* **2023**, *19*, 2305104. [CrossRef] [PubMed]
94. Moradi, A.; Szewczyk, P.K.; Roszko, A.; Fornalik-Wajs, E.; Stachewicz, U. Unraveling the impact of boron nitride and silicon nitride nanoparticles on thermoplastic polyurethane fibers and mats for advanced heat management. *ACS Appl. Mater. Interfaces* **2024**, *16*, 41475–41486. [CrossRef] [PubMed]
95. Jones, R.S.; Gonzalez-Munoz, S.; Griffiths, I.; Holdway, P.; Evers, K.; Luanwuthi, S.; Maciejewska, B.M.; Kolosov, O.; Grobert, N. Thermal conductivity of carbon/boron nitride heteronanotube and boron nitride nanotube buckypapers: Implications for thermal management composites. *ACS Appl. Nano Mater.* **2023**, *6*, 15374–15384. [CrossRef] [PubMed]
96. Ovchinnikov, I.S.; Vishnevskiy, A.S.; Seregin, D.S.; Rezvanov, A.A.; Schneider, D.; Sigov, A.S.; Vorotilov, K.A.; Baklanov, M.R. Evaluation of mechanical properties of porous OSG films by PFQNM AFM and benchmarking with traditional instrumentation. *Langmuir* **2020**, *36*, 9377–9387. [CrossRef]
97. Abdelhady, H.G.; Abdel-Salam, H.A.; Niazy, E.M.; Mueller, A.; Quast, M.J.; Effat, A.M.; Elbehairi, S.-E. Spatiotemporal PFQNM visualization of the effect of suicide dendriplexes on dividing HeLa cells. *Nanomed. Nanotechnol. Biol. Med.* **2016**, *12*, 2365–2371. [CrossRef]
98. Papi, M.; Paoletti, P.; Geraghty, B.; Akhtar, R. Nanoscale characterization of the biomechanical properties of collagen fibrils in the sclera. *Appl. Phys. Lett.* **2014**, *104*, 103703. [CrossRef]
99. Li, J.; Mathew, A.P. Effect of decoration route on the nanomechanical, adhesive, and force response of nanocelluloses—An in-situ force spectroscopy study. *PLoS ONE* **2022**, *18*, e0279919. [CrossRef]
100. Mendes, A.C.; Sevilla Moreno, J.; Hanif, M.; Douglas, T.E.L.; Chen, M.L.; Chronakis, I.S. Morphological, mechanical and mucoadhesive properties of electrospun chitosan/phospholipid hybrid nanofibers. *Int. J. Mol. Sci.* **2018**, *19*, 2266. [CrossRef]
101. Liu, L.L.; Chen, S.X.; Xu, A.C.; Cai, G.M. Manufacturing high sensitive strain sensor of polyurethane nanofiber mat/AgNWs by simple dip-dry method. *Fibers Polym.* **2020**, *21*, 359–365. [CrossRef]
102. Zarei, M.; Samimi, A.; Khorram, M.; Abdi, M.M.; Golestaneh, S.I. Fabrication and characterization of conductive polypyrrole/chitosan/collagen electrospun nanofiber scaffold for tissue engineering application. *Int. J. Biol. Macromol.* **2021**, *168*, 175–186. [CrossRef] [PubMed]
103. Wang, S.S.; Huang, J.; Zhang, X.; Zhang, J.B. Direct measurement of proton conductivity of a single ionomer nanofiber. *Nano Energy* **2022**, *102*, 107738. [CrossRef]

104. Sengupta, D.; Chen, S.-H.; Michael, A.; Kwok, C.Y.; Lim, S.; Pei, Y.T.; Prakash Kottapalli, A.G. Single and bundled carbon nanofibers as ultralightweight and flexible piezoresistive sensors. *npj Flex. Electron.* **2020**, *4*, 9. [CrossRef]
105. Mondal, K.; Maitra, T.; Srivastava, A.K.; Pawar, G.; McMurtrey, M.D.; Sharma, A. Particle size effect on enhanced graphitization and electrical conductivity of suspended gold/carbon composite nanofibers. *Ind. Eng. Chem. Res.* **2020**, *59*, 1944–1952. [CrossRef]
106. Serrano-Garcia, W.; Ramakrishna, S.; Thomas, S.W. Electrospinning technique for fabrication of coaxial nanofibers of semiconductive polymers. *Polymers* **2022**, *14*, 5073. [CrossRef]
107. Lee, J.Y.; Kang, T.-H.; Choi, J.H.; Yu, W.-R. Improved electrical conductivity of poly(ethylene oxide) nanofibers using multi-walled carbon nanotubes. *AIP Adv.* **2018**, *8*, 035024. [CrossRef]
108. Koderman Podborsek, G.; Zupancic, S.; Kaufman, R.; Surca, A.K.; Marsel, A.; Pavlixic, A.; Hodnik, N.; Drazic, G.; Bele, M. Microstructure and electrical conductivity of electrospun titanium oxynitride carbon composite nanofibers. *Nanomaterials* **2022**, *12*, 2177. [CrossRef]
109. Henrichsen, H.H.; Kjelstrup-Hansen, J.; Engstrom, D.; Clausen, C.H.; Boggild, P.; Rubahn, H.-G. Electrical conductivity of organic single-nanofiber devices with different contact materials. *Org. Electron.* **2007**, *8*, 540–544. [CrossRef]
110. Qi, H.N.; Wang, G.Y.; Hu, Y.L.; Shao, H.; Ma, Q.L.; Li, D.; Yu, W.S.; Chang, L.M.; Zhang, X.J.; Dong, X.T. Conjugate electro-spinning towards Janus nanofibers array synchronously endowed with conductive anisotropy, magnetism and luminescence. *Mater. Today Comm.* **2022**, *33*, 104765. [CrossRef]
111. El-Ghazali, S.; Kobayashi, H.; Khatri, M.; Phan, D.-N.; Khatri, Z.; Mahar, S.K.; Kobayashi, S.; Kim, I.-S. Preparation of a Cage-Type Polyglycolic Acid/Collagen Nanofiber Blend with Improved Surface Wettability and Handling Properties for Potential Biomedical Applications. *Polymers* **2021**, *13*, 3458. [CrossRef]
112. Shi, T.T.; Liu, Y.; Wang, D.H.; Xia, D.; Li, B.; Xu, R.D.; Li, N.; Liang, C.Y.; Chen, M.L. Spatially engineering tri-layer nanofiber dressings featuring asymmetric wettability for wound healing. *Nano Mater. Sci.* **2024**, *in press*. [CrossRef]
113. Schoolaert, E.; Cossu, L.; Becelaere, J.; van Guyse, J.F.R.; Tigrine, A.; Vergaelen, M.; Hoogenboom, R.; de Clerck, K. Nanofibers with a tunable wettability by electrospinning and physical crosslinking of poly(2-*n*-propyl-2-oxazoline). *Mater. Des.* **2020**, *192*, 108747. [CrossRef]
114. Jalali, S.; Kruppke, I.; Enghardt, S.; Wiesmann, H.-P.; Kruppke, B. Silica nanofibers with enhanced wettability and mechanical strength for bone tissue engineering: Electrospinning without polymer carrier and subsequent heat treatment. *Macromol. Mater. Eng.* **2024**, *309*, 2300169. [CrossRef]
115. Wu, H.; Zhang, R.; Sun, Y.; Lin, D.D.; Sun, Z.Q.; Pan, W.; Downs, P. Biomimetic nanofiber patterns with controlled wettability. *Soft Matter* **2008**, *4*, 2429–2433. [CrossRef]
116. Bagrov, D.; Perunova, S.; Pavlova, E.; Klinov, D. Wetting of electrospun nylon-11 fibers and mats. *RSC Adv.* **2021**, *11*, 11373–11379. [CrossRef]
117. Andrade, K.L.; Faita, F.L.; do Nascimento, R.M.; Sousa Cunha, R.; Bresolin, D.; Diz Acosta, E.; Machado, R.A.F. Wettability tuning of natural rubber/polyvinylpyrrolidone electrospun nonwoven mats. *Surf. Interfaces* **2022**, *32*, 102129. [CrossRef]
118. Alam, A.K.M.M.; Ewaldz, E.; Xiang, C.H.; Qu, W.D.; Bai, X.L. Tunable wettability of biodegradable multilayer sandwich-structured electrospun nanofibrous membranes. *Polymers* **2020**, *12*, 2092. [CrossRef]
119. Heinz, M.; Chowdhury, I.U.; Stephan, P.; Gambaryan-Roisman, T. Water drops on nanofiber-coated substrates: Influence of wall temperature and coating thickness on hydrodynamics and wall heat flux distribution. *Int. J. Heat Mass Transf.* **2024**, *222*, 125117. [CrossRef]
120. Shi, J.; Li, S.-F.; Feng, K.; Han, S.-Y.; Hu, T.-G.; Wu, H. Improving the viability of probiotics under harsh conditions by the formation of biofilm on electrospun nanofiber mat. *Foods* **2022**, *11*, 1203. [CrossRef]
121. Nitti, P.; Gallo, N.; Palazzo, B.; Sannino, A.; Polini, A.; Verri, T.; Barca, A.; Gervaso, F. Effect of L-Arginine treatment on the *in vitro* stability of electrospun aligned chitosan nanofiber mats. *Polym. Test.* **2020**, *91*, 106758. [CrossRef]
122. Bekou, S.; Mattia, D. Wetting of nanotubes. *Curr. Opin. Colloid Interface Sci.* **2011**, *16*, 259–265. [CrossRef]
123. Neimark, A.V. Thermodynamic equilibrium and stability of liquid films and droplets on fibers. *J. Adhes. Sci. Technol.* **1999**, *13*, 1137–1154. [CrossRef]
124. Barber, A.H.; Cohen, S.R.; Wagner, H.D. External and internal wetting of carbon nanotubes with organic liquids. *Phys. Rev. B* **2005**, *71*, 115443. [CrossRef]
125. Gambaryan-Roisman, T. Liquids on porous layers: Wetting, imbibition and transport processes. *Curr. Opin. Colloid Interface Sci.* **2014**, *19*, 320–335. [CrossRef]
126. Yum, K.S.; Yu, M.-F. Measurement of wetting properties of individual boron nitride nanotubes with the wilhelmy method using a nanotube-based force sensor. *Nano Lett.* **2006**, *6*, 329–333. [CrossRef] [PubMed]
127. Stachewicz, U.; Barber, A.H. Enhanced wetting behavior at electrospun polyamide nanofiber surfaces. *Langmuir* **2011**, *27*, 3024–3029. [CrossRef]
128. Wang, J.; Anthony, D.B.; Fuentes, C.A.; De Luca, H.G.; Zhang, D.X.; Bismarck, A.; van Vuure, A.W.; Shaffer, M.S.P.; Seveno, D. Wettability of carbon nanotube-grafted carbon fibers and their interfacial properties in polypropylene thermoplastic composite. *Compos. Part A: Appl. Sci. Manuf.* **2022**, *159*, 106993. [CrossRef]
129. Barber, A.H.; Cohen, S.R.; Wagner, H.D. Static and dynamic wetting measurements of single carbon nanotubes. *Phys. Rev. Lett.* **2004**, *92*, 186103. [CrossRef] [PubMed]

130. Stachewicz, U.; Stone, C.A.; Willis, C.R.; Barber, A.H. Charge assisted tailoring of chemical functionality at electrospun nanofiber surfaces. *J. Mater. Chem.* **2012**, *22*, 22935–22941. [CrossRef]
131. Stachewicz, U.; Bailey, R.J.; Zhang, H.; Stone, C.A.; Willis, C.R.; Barber, A.H. Wetting hierarchy in oleophobic 3D electrospun nanofiber networks. *ACS Appl. Mater. Interfaces* **2015**, *7*, 16645–16652. [CrossRef]
132. Yazdanpanah, M.M.; Hosseini, M.; Pabba, S.; Berry, S.M.; Dobrokhotov, V.V.; Safir, A.; Keynton, R.S.; Cohn, R.W. Micro-Wilhelmy and related liquid property measurements using constant-diameter nanoneedle-tipped atomic force microscope probes. *Langmuir* **2008**, *24*, 13753–13764. [CrossRef] [PubMed]
133. Wu, S.-H.; Qin, X.-H. Effects of the stabilization temperature on the structure and properties of polyacrylonitrile-based stabilized electrospun nanofiber microyarns. *J. Therm. Anal. Calorim.* **2013**, *116*, 303–308. [CrossRef]
134. Duan, G.G.; Fang, H.; Huang, C.B.; Jiang, S.H.; Hou, H.Q. Microstructures and mechanical properties of aligned electrospun carbon nanofibers from binary composites of polyacrylonitrile and polyamic acid. *J. Mater. Sci.* **2018**, *53*, 15096–15106. [CrossRef]
135. Storck, J.L.; Wortmann, M.; Brockhagen, B.; Frese, N.; Diestelhorst, E.; Grothe, T.; Hellert, C.; Ehrmann, A. Comparative study of metal substrates for improved carbonization of electrospun PAN nanofibers. *Polymers* **2022**, *14*, 721. [CrossRef] [PubMed]
136. Tan, E.P.S.; Goh, C.N.; Sow, C.H.; Lim, C.T. Tensile test of a single nanofiber using an atomic force microscope tip. *Appl. Phys. Lett.* **2005**, *86*, 073115. [CrossRef]
137. Zou, Y.; Jiang, S.H.; Hu, X.W.; Xu, W.H.; Chen, Z.G.; Liu, K.M.; Hou, H.Q. Influence of pre-oxidation on mechanical properties of single electrospun polyacrylonitrile nanofiber. *Mater. Today Comm.* **2021**, *26*, 102069. [CrossRef]
138. Hwang, K.Y.; Kim, S.-D.; Kim, Y.-W.; Yu, W.-R. Mechanical characterization of nanofibers using a nanomanipulator and atomic force microscope cantilever in a scanning electron microscope. *Polym. Test.* **2010**, *29*, 375–380. [CrossRef]
139. Alharbi, N.; Daraei, A.; Lee, H.S.; Guthold, M. The effect of molecular weight and fiber diameter on the mechanical properties of single, electrospun PCL nanofibers. *Mater. Today Comm.* **2023**, *35*, 105773. [CrossRef]
140. Sharpe, J.M.; Lee, H.S.; Hall, A.R.; Bonin, K.; Guthold, M. Mechanical properties of electrospun, blended fibrinogen: Pcl nanofibers. *Nanomaterials* **2020**, *10*, 1843. [CrossRef]
141. Baker, S.R.; Banerjee, S.; Bonin, K.; Guthold, M. Determining the mechanical properties of electrospun poly-ε-caprolactone (PCL) nanofibers using AFM and a novel fiber anchoring technique. *Mater. Sci. Eng. C* **2016**, *59*, 203–212. [CrossRef]
142. Parvej, M.S.; Wang, X.N.; Jiang, L. AFM based nanomechanical characterization of cellulose nanofibril. *J. Comp. Mater.* **2020**, *54*, 4487–4493. [CrossRef]
143. Bidhar, S.; Goss, V.; Chen, W.-Y.; Stanishevsky, A.; Li, M.M.; Kuksenko, S.; Calviani, M.; Zwaska, R. Production and qualification of an electrospun ceramic nanofiber material as a candidate future high power target. *Phys. Rev. Accel. Beams* **2021**, *24*, 123001. [CrossRef]
144. Bulbul, Y.E.; Uzunoglu, T.; Dilsiz, N.; Yildirim, E.; Ates, H. Investigation of nanomechanical and morphological properties of silane-modified halloysite clay nanotubes reinforced polycaprolactone bio-composite nanofibers by atomic force microscopy. *Polym. Test.* **2020**, *92*, 106877. [CrossRef]
145. Cheng, Q.Z.; Wang, S.Q. A method for testing the elastic modulus of single cellulose fibrils via atomic force microscopy. *Compos. Part A Appl. Sci. Manuf.* **2008**, *39*, 1838–1843. [CrossRef]
146. Kontomaris, S.V.; Stylianou, A.; Chliveros, G.; Malamou, A. Overcoming challenges and limitations regarding the atomic force microscopy imaging and mechanical characterization of nanofibers. *Fibers* **2023**, *11*, 83. [CrossRef]
147. Biagi, G.; Holmgaard, T.; Skovsen, E. Near-field electrospinning of dielectric-loaded surface plasmon polariton waveguides. *Opt. Express* **2013**, *21*, 4355–4360. [CrossRef] [PubMed]
148. Caldiroli, A.; Cappelletti, S.; Birarda, G.; Redaelli, A.; Riboldi, S.A.; Stani, C.; Vaccari, L.; Piccirilli, F. Infrared nanospectroscopy depth-dependent study of modern materials: Morpho-chemical analysis of polyurethane/fibroin binary meshes. *Analyst* **2023**, *48*, 3584–3593. [CrossRef]
149. Beermann, J.; Bozhevolnyi, S.I.; Balzer, F.; Rubahn, H.-G. Two-photon near-field mapping of local molecular orientations in hexaphenyl nanofibers. *Laser Phys. Lett.* **2005**, *2*, 480–484. [CrossRef]
150. Richard-Lacroix, M.; Pellerin, C. Orientation and structure of single electrospun nanofibers of poly(ethylene terephthalate) by confocal raman spectroscopy. *Macromolecules* **2012**, *45*, 1946–1953. [CrossRef]
151. Bellan, L.M.; Craighead, H.G. Molecular orientation in individual electrospun nanofibers measured via polarized Raman spectroscopy. *Polymer* **2008**, *49*, 3125–3129. [CrossRef]
152. Sfakis, L.; Sharikova, A.; Tuschel, D.; Costa, F.X.; Larsen, M.; Khmaladze, A.; Castracane, J. Core/shell nanofiber characterization by Raman scanning microscopy. *Biomed. Opt. Express* **2017**, *8*, 1025–1035. [CrossRef] [PubMed]
153. Kharinthsev, S.S.; Saparina, S.V.; Fishman, A.I.; Stolov, A.A.; Li, J. Spectrally resolving coherent TERS spectroscopy of electrically biased carbon-coated fibers. *J. Phys. Chem. C* **2020**, *124*, 14752–14758. [CrossRef]
154. Chaunchaiyakul, S.; Yano, T.; Khoklang, K.; Krukowski, P.; Akai-Kasaya, M.; Saito, A.; Kuwahara, Y. Nanoscale analysis of multiwalled carbon nanotube by tip-enhanced Raman spectroscopy. *Carbon* **2016**, *99*, 642–648. [CrossRef]